Solution and Extension of a New Benchmark Problem for Eddy Current Nondestructive Testing

L. Barbato[1], N. Poulakis[2], A. Tamburrino[1,3], and T. Theodoulidis[4], S. Ventre[1]

[1]DIEI, Università di Cassino e del Lazio Meridionale, Cassino, 03043 Italy
[2]Department of Electrical Engineering, TEI of Western Macedonia, Kozani, 50100 Greece
[3]Nondestructive Evaluation Laboratory, Michigan State University, East Lansing, Michigan 48824, USA
[4]Department of Mechanical Engineering, University of Western Macedonia, Kozani, 50100 Greece

We report on further measurements and a numerical solution for a proposed benchmark problem involving an eddy current nondestructive evaluation configuration. This is a simplified version of the inspection of fastener holes in aircraft structures, comprising combinations of plates with through holes and a crack. Previously only line (B-scan) data were provided for the coil impedance while in this follow-up work we provide precision surface (C-scan) data as well as details on the evaluation of the critical parameters of the problem. Furthermore, the experimental data are cross-validated with numerical ones by using a model that combines an integral/FEM approach.

***Index Terms*— Benchmark testing, eddy currents, impedance measurement, nondestructive testing.**

I. Introduction

EDDY current testing is an established NonDestructive Testing (NDT) method that is routinely used in a number of important applications ranging from the tube inspection in nuclear power plant steam generators to structural integrity checks of commercial and/or military aircrafts [1]. For the latter, the inspection and location of cracks adjacent to aluminum fastener holes is of great interest since the development and propagation of such fatigue cracks may have detrimental effects on the structural integrity of the aircraft [2]. All NDE methods involve the interaction of some form of energy with the inspected testpiece and the monitoring of this interaction with appropriate sensors. In the case of eddy current testing it is the magnetic field coupling of an inspection coil and the alteration of the eddy current flow around the defect/crack. In the classical approach, this is monitored by the impedance of the coil and its change as the coil is moved above the testpiece area with the defect/crack. There are various issues in this procedure and computer modeling plays an important role like in the optimization of the probe coil shape, the excitation frequency selection, the interpretation of results, the imaging of cracks, etc.

The basic simulation setup involves a large testpiece, a coil excited by a frequency of the order of kHz and a discontinuity in the testpiece in the form of a volume defect or a surface like crack. Because the defect is usually much smaller than the testpiece and/or the coil, modeling constitutes a multi-scale problem, i.e. the field perturbations and defect signals are weak compared to the ones produced by the coil and the conductor. In addition, narrow cracks or small lift-offs (distance of coil from testpiece) are usually present and affect mesh quality [3]. Integral equation methods are commonly used, but the need for dedicated Green's functions with analytical expressions that correspond to the specific conductor geometries limit their scope [4-6]. In this work a source integral equation method is adopted where the unknown is the induced current density. The underlying integral equation is solved by discretizing the unknown by means of Whitney forms and applying the Galerkin method [7]. The advantages of this approach are the need of discretizing the material regions only, the numerical integration of a kernel that is singular ($1/r$) but not hypersingular, the possibility of treating arbitrary geometries and materials (possibly inhomogeneous and/or anisotropic [8]) and the no need to impose explicitly the regularity conditions at infinite. The main drawback is the need of storing $O(N^2)$ and inverting a fully populated matrix ($O(N^3)$ with a direct method). Despite of this, compression methods for reducing the memory occupancy (almost $O(N)$) and fast solvers for reducing the solution time to about $O(N^2)$ have been recently developed [9], [10]. Moreover, an ad-hoc variant of this numerical model has been specifically tailored for fast and accurate computations in eddy current testing applications [11].

All solution methods and available codes require validation which is usually performed by comparing theoretical results to precision measurements taken from well prepared experiments. A review of existing benchmark configurations was provided in [13] with special emphasis and critical comments on the data-sets and characteristics of the TEAM Workshop No.8, 15 and 27 problems. Also in [13], a new benchmark problem was proposed that consisted of a set of plates with through-wall holes and a crack. Four combinations of testing configurations were created by arranging the plates and precision coil impedance measurements were reported. The proposed problem can be regarded as a canonical one and represents a simplified version of the eddy current

Manuscript received September 10, 2014. Corresponding author: A. Tamburrino (e-mail: tamburrino@unicas.it).
DOI: 10.1109/TMAG.2015.2406765

nondestructive inspection of fastener holes in aircraft structures.

The purpose of the current work is twofold: (i) to considerably enrich the data of that benchmark problem by providing additional surface (C-scans) of the coil impedance and (ii) to provide numerical results by using a model that combines an integral/FEM approach.

II. Benchmark Problem Description

A detailed description of the problem configuration was given in [13] and repeated here. Two aluminum plates were used in the experiments to simulate a layered structure. Both of them had dimensions 300×300 mm, a thickness of 2 mm and a through-hole at the center of their area. In addition, one of them had a narrow, through slot simulating a crack adjacent to the hole and in a radial direction with respect to it. If we designate the plate without the crack as A and the one with the crack as B, we have performed measurements for the following 4 configurations that are named depending on the plate(s) used and their position when stuck together:

A : plate-A alone (no crack)
B : plate-B alone (through the thickness crack)
AB : plate-A placed above plate-B (bottom layer crack)
BA : plate-B placed above plate-A (top layer crack)

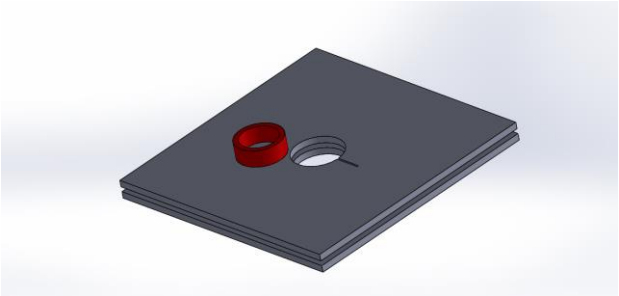

Fig. 1. Experimental setup for one of the configurations (BA).

The narrow slot was made by Electro Discharge Machining (EDM) while the coil was constructed by layer-winding copper wire (0.1 mm diameter) onto a suitable Delrin former. The coil impedance data were recorded by using the precision LCR meter Agilent 4284A (precision 0.05%) at two frequencies, 1 and 5 kHz. The coil and plate parameters are shown in Table I. For the specific plates' conductivity, these frequencies correspond to skin depths of 3.82 and 1.71 mm, respectively.

TABLE I
TEST SETUP PARAMETERS

COIL	M1650	PLATE(S)	A and B
Inner radius	7.0 mm	Thickness	2 mm
Outer radius	12.0 mm	Conductivity	17.34 MS/m
Height	4.0 mm	Rel.Permeability	1
Wire-turns	1650	Gap between	70 μm
Lift-off	1.082 mm	Hole radius	10.0 mm
L_0 (measured)	53.655 mH	Crack length/width	9.8/0.234 mm

One of the experimental setups (BA) is shown in Fig.1. A Cartesian coordinate system is associated to the geometry. The surface of the top plate coincides with the plane O*xy*, the hole's with the coordinate system center and the crack line with the *x*-axis. The data were collected as a function of coil position and for that matter an XY translation stage was used (controlled by a PC, position accuracy 0.05 mm), which correlated the position of the coil with the measured data. Instead of mounting the coil onto the moveable part of the XY stage, it was fixed and the test object was moved under it.

III. Experimental Results

The impedance values were acquired by averaging 16 measurements for each coil position and frequency. First, the inductance of the coil in air was measured to the value shown in Table I as follows. A frequency scan is performed with the coil away from any conductive structure, the results are shown in Fig.2. A typical L_0 vs frequency curve has a straight part that spans a frequency range, a diminish part due to the measuring instrument accuracy deterioration at lower frequencies and an upward range at higher frequencies where capacitive effects start to be important. These are due to the distributed capacitance between the coil wires and the capacitance associated with the coil leads and for even higher frequencies they become predominant and the coil reaches resonance. As pointed out in [14], a safe measurement range, that is a range where the experimental results can be safely compared to theoretical ones spans to a frequency as high as one-tenth of the specific coil resonance frequency, while by following the correction procedure, this safe measurement range can be increased up to half of the resonance frequency. In our case, however, such a correction procedure was not necessary since the frequencies were much lower than the resonance frequency of the coil.

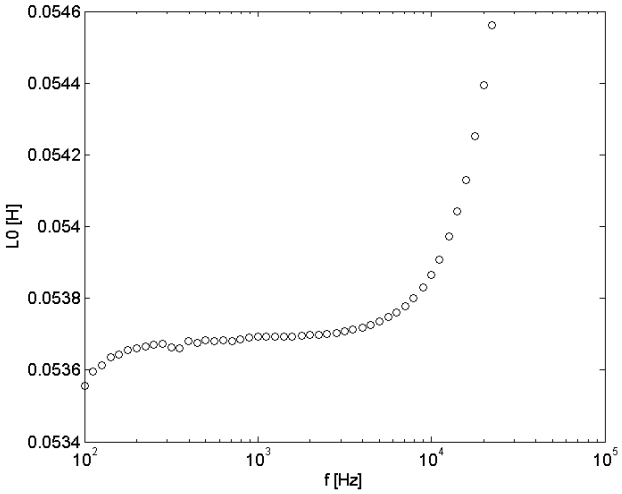

Fig. 2. Experimental measurements showing variation of coil inductance with frequency.

The inductance of the coil in air was computed to 54.139 mH, by using the well established Dodd and Deeds model [15-16], thus giving a discrepancy of 0.9% with respect to the measured value. This small discrepancy can be attributed to the fact that the theoretical model assumes that the coil is an ideal conductor carrying a uniform distributed current. In [14],

an effective value for the outer coil radius was established, in order to get a perfect match between the measured and the theoretical value. In our case, this would result to a value of 6.938 mm instead of 7 mm, which is less than a single wire diameter and would therefore represent a legitimate correction. However, this was not considered necessary and, instead, we followed the usual approach of presenting the results in normalized form, the normalization factor being the coil reactance $X_0=2\pi fL_0$ in air [1]. Hence, when comparing the experimental data to theoretical results, by normalizing with the corresponding experimental or theoretical X_0, it is expected that small dimensional deviations will not affect agreement between them.

Initially, the lift-off was measured with a micrometer and the conductivity with the GE Phasec 2D instrument working in conductivity mode. For greater accuracy, effective values for the lift-off and the conductivity were determined by following the standard method [14], which involves the minimization of the RMS error between the experimental impedance and the theoretical calculations over a frequency range for the coil above each plate and away from the hole and crack. The theoretical model used in this case was again the Dodd and Deeds model [15, 16].

Fig.3 shows the normalized impedance data arising from a frequency scan together with the theoretical data for the values of lift-off and conductivity shown in Table I. In general the variation of the lift-off moves the arc-shape curve inwards for increasing lift-off and outwards for decreasing lift-off while the variation of the conductivity moves the data points on the curve upwards (for decreasing conductivity) or downwards along the curve (for increasing conductivity).

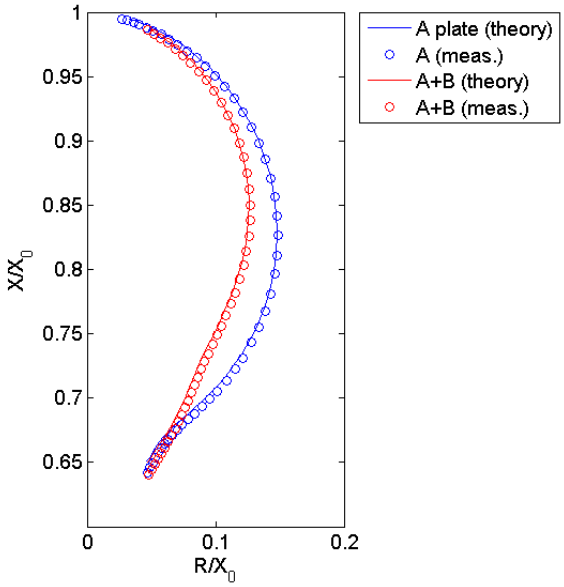

Fig. 3. Variation of coil inductance with frequency. Comparison of experimental measurements to theoretical results.

In all cases, a C-scan was performed, i.e. the coil was moved above the hole with or without the crack in a raster of measurement points covering an area of 150×150 mm at maximum. In the direction of the crack (*x*-axis) the step was set to 1 mm while in the perpendicular direction (*y*-axis) it was set to 2 mm. Representative experimental results are presented next for the precision impedance measurements for each of the four configurations.

IV. The Numerical Model

The numerical model used through this paper is derived from [7] and described in [11]. It is also at the basis of a new prototypal plug-in recently developed for the CIVA software [17] within the framework of an European (FP7) founded project (SIMPOSIUM project) [19]. It is optimized for typical eddy current testing scenarios which are multiscale: the unperturbed (no defects are present) eddy current $\mathbf{J}_0$ generated by the driving coil is distributed on a large region and on a coarse scale, whereas the perturbation $\delta\mathbf{J}$ of the eddy current density due to a "small" defect is concentrated in a neighborhood of the defect and its spatial scale is definitely finer than those of the unperturbed field. A discretization of the complete problem, i.e. computing the induced eddy current $\mathbf{J}=\mathbf{J}_0+\delta\mathbf{J}$ in the presence of the defect, would require an extended and finer mesh to accomplish the requirements of an appropriate discretization for both $\mathbf{J}_0$ and $\delta\mathbf{J}$ at the same time. Therefore the number of elements could become prohibitively high. The approach followed in the CARIDDI_ECT code [11, 12] is to compute separately $\mathbf{J}_0$ and $\delta\mathbf{J}$ on two different finite element meshes optimized for each sub-problem. This strategy is very effective especially when the solution of the forward problem has to be computed on several/many different defect geometries (as is the case when solving the inverse problem through an iterative method or generating a database, etc.)

This numerical model, combines the integral/FEM approaches and is based on the following integral equations (linear constitutive relationships, non magnetic materials and time-harmonic operations):

$$\eta\delta\mathbf{J} + i\omega\mathbf{A}[\delta\mathbf{J}] + \nabla\delta\varphi = \mathbf{0} \quad \text{in } \Omega_{BG} \tag{1}$$

subject to

$$\delta\mathbf{J} = -\mathbf{J}_{BG} \quad \text{in } \Omega_{BG} \tag{2}$$

where η is the electric resistivity, ω is the angular frequency, $\delta\mathbf{J}$ and $\delta\varphi$ are the perturbations of the eddy currents and scalar potential due to perfectly insulating defect Ω hosted in the background domain Ω_{BG} $(\Omega \subset \Omega_{BG})$, $\mathbf{A}[\cdot]$ is the operator giving the vector potential due to prescribed sources

$$\mathbf{A}:\mathbf{u}(\mathbf{r}) \rightarrow \frac{\mu_0}{4\pi}\iiint_{\Omega_{BG}} \frac{\mathbf{u}(\mathbf{r}')}{|\mathbf{r}-\mathbf{r}'|}dV' \quad \forall \mathbf{r} \in \Omega_{BG} \tag{3}$$

and $\mathbf{J}_{BG}$ is the eddy current density in the absence of the anomaly. The formulation is "optimized" in the sense that the unknown $\delta\mathbf{J}$ is "localized" in the neighbourhood of the defect Ω. The proper functional space for $\delta\mathbf{J}$ is

$$J = \{\mathbf{u} \in H(div, \Omega_{BG}) \mid \nabla\cdot\mathbf{u} = 0, \mathbf{u}\cdot\hat{\mathbf{n}} = 0 \text{ on } \partial\Omega_{BG}\} \tag{4}$$

The corresponding weak forms of the equations (1) and (2) are hereafter reported (explicated according to Galerkin's method)[1]:

$$\iiint_{\Omega_{BG}} \{\eta\delta\mathbf{J}(\mathbf{r}') + i\omega\mathbf{A}[\delta\mathbf{J}(\mathbf{r}')]\} \cdot \delta\mathbf{J}(\mathbf{r}')dV' = \mathbf{0} \quad \text{in } \Omega_{BG} \tag{5}$$

and

$$\iiint_{\Omega} [\delta\mathbf{J}(\mathbf{r}') + \mathbf{J}_{BG}(\mathbf{r}')] \cdot \delta\mathbf{J}(\mathbf{r}')dV' = \mathbf{0} \quad \text{in } \Omega \tag{6}$$

The unknown is discretized as $\delta\mathbf{J} = \sum_k \delta I_k \nabla \times \mathbf{N}_k(\mathbf{r})$ where the $\mathbf{N}_k$'s are edge-element-based shape functions [7]. Suitable conditions guarantee the uniqueness of the solution as well as the condition $\delta\mathbf{J} \cdot \hat{\mathbf{n}} = 0$ on $\partial\Omega_{BG}$ in weak form.

By combining the above discretization and the weak form (5) and (6) we obtain the following discretized model:

$$\underline{\underline{K}}^T \underline{\underline{Z}}\underline{\underline{K}}\underline{x} = -\underline{\underline{K}}^T \underline{\underline{Z}}\underline{a}_0 \tag{7}$$

where $\underline{\underline{Z}} = \underline{\underline{L}} + i\omega\underline{\underline{R}}$ (matrices $\underline{\underline{L}}$ and $\underline{\underline{R}}$ are defined in [7]) and the matrix $\underline{\underline{K}}$ and the column vector $\underline{a}_0$ are defined in [11]. Eventually $\delta\underline{I}$, the column vector of Degree of Freedom δI_k's, can be computed from $\underline{x}$ as $\delta\underline{I} = \underline{\underline{K}}\underline{x} + \underline{a}_0$ [11]. It can be proven that $\underline{\underline{K}}\underline{x}$ represents current density vanishing in the region occupied by the defect Ω, regardless the value of the column vector $\underline{x}$ [11].

V. Numerical results

In this section we report results concerning the validation of the experimental data relative to the proposed benchmark problem. For all the cases, the numerical results (impedance variations) are compared to the experimental data, according to the common NDT data presentations (B-scan and/or C-scan) or in the complex plane (appropriate for eddy current testing). The B-scan representation covers a line of 90mm (passing at $y = 0$) with a step of 1 mm, while the C-scan representation covers an area of 30×30 mm^2, with a step of 1 mm in the x direction (parallel to the crack) and 2 mm in the y direction (orthogonal to the crack). In both representations, the centre of the hole is located at the origin of the reference system. The results are normalized with respect to the value of the reactance of the probe in air and evaluated at the frequencies of 1 kHz and 5 kHz.

The first validation is related to Case A (Plate A). Fig.4 shows the comparison between the numerical and experimental data in the B-scan representation, as well as the complex impedance curves. In both cases, the agreement between the numerical and experimental data is excellent.

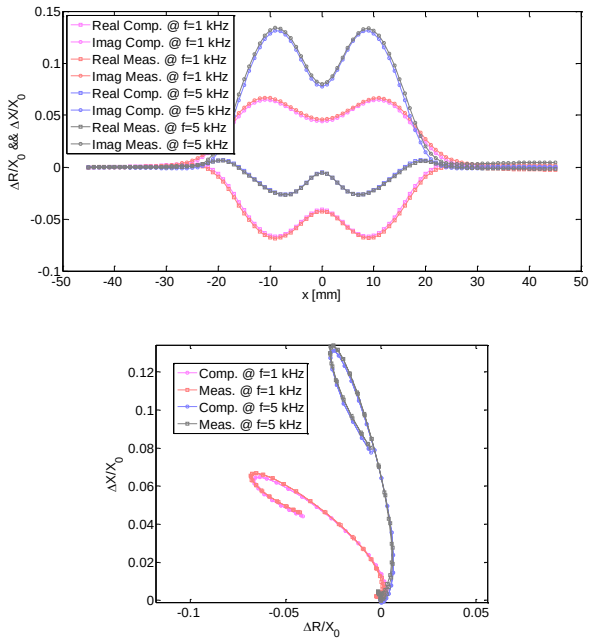

Fig. 4. Case A – Comparison between the experimental and numerically computed data at 1 kHz and 5 kHz. Top: B-scan, bottom: complex plane presentation.

The second case is B (Plate B). Fig. 5 shows the numerically computed impedance variation vs the experimental one. A C-scan representation of the difference between the experimental (Fig. 6) and numerically computed magnitude of the impedance is shown in Fig. 7. Also in this case the agreement is excellent: the ratio between the maximum of the difference and the maximum of the magnitude of the numerically computed impedance is 9.72×10^{-3} and 7.06×10^{-3} for 1 kHz and 5 kHz, respectively.

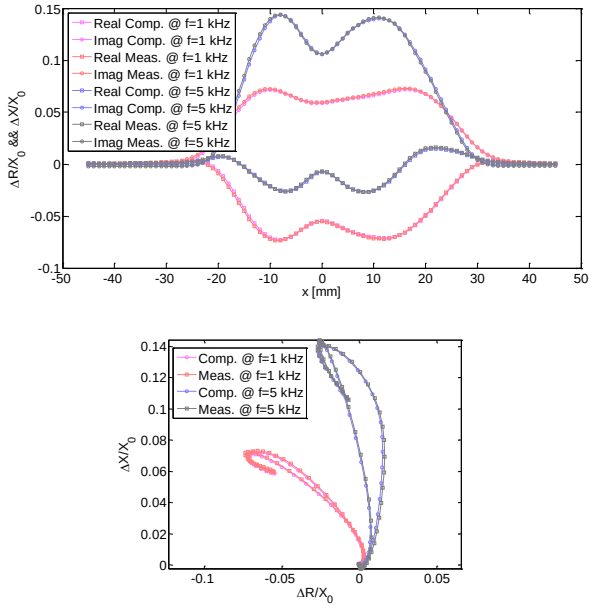

Fig. 5. Case B – Comparison between the experimental and numerically computed data at 1 kHz and 5 kHz. Top: B-scan, bottom: complex plane representation.

[1]The $\nabla\delta\varphi$ contribute disappears in the weak formulation.

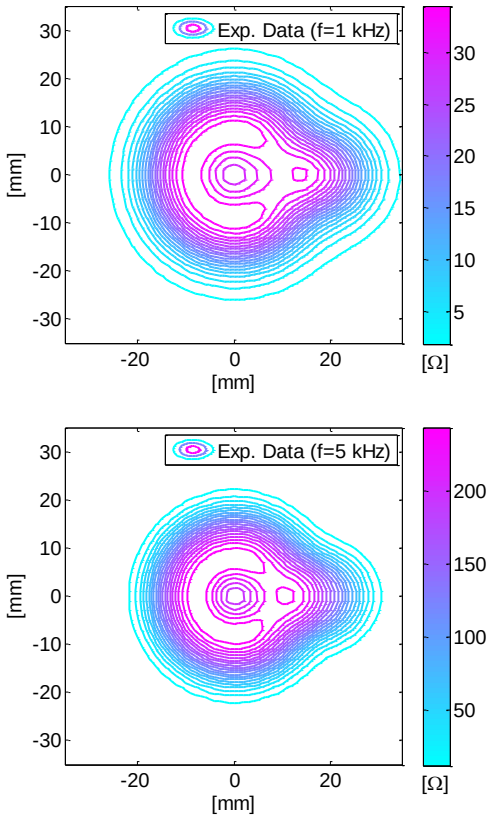

Fig. 6. Case B - C-scan representation of the experimental impedance variation at 1 kHz and 5 kHz.

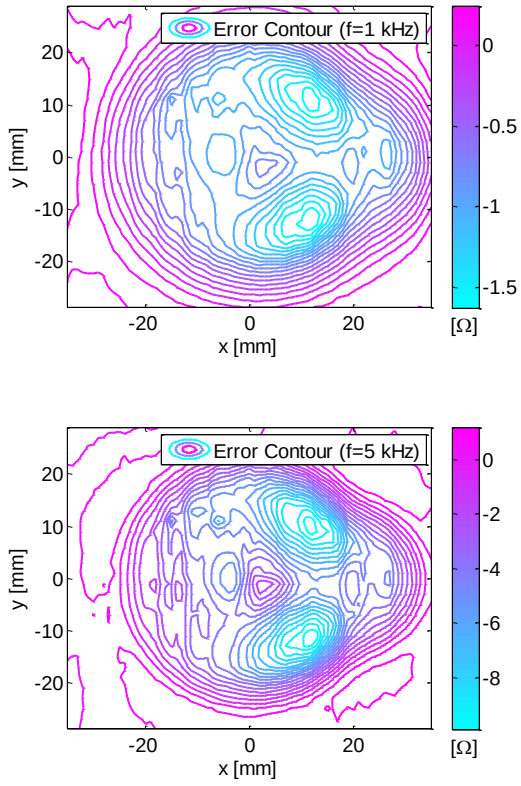

Fig. 7. Case B - C-scan representation of the difference between the experimental and numerical impedance variation at 1 kHz and 5 kHz.

The third validation is relative to the Case AB that includes the two plates A and B in a configuration where plate A overlaps plate B; the gap between them is 70 μm. Fig. 8 shows the comparison of the experimental and numerical data according to the coil position and also depicts the relevant complex impedance curves. A C-scan representation of the difference between the numerically computed and

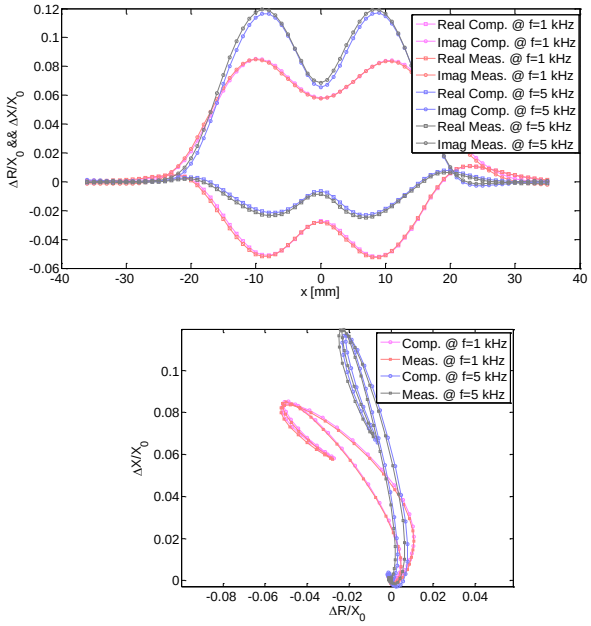

Fig. 8. Case AB – Comparison between the experimental and numerically computed data at 1 kHz and 5 kHz. Top: B-scan, bottom: complex plane representation.

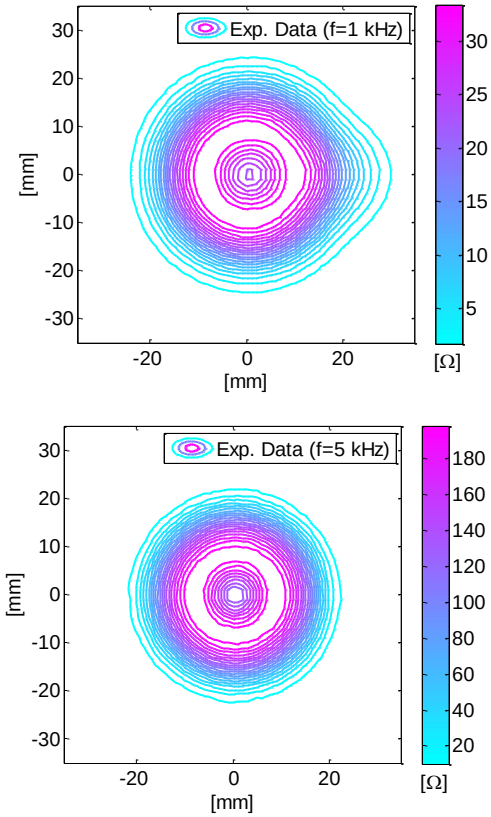

Fig. 9. Case AB - C-scan representation of the experimental impedance variation at 1 kHz and 5 kHz.

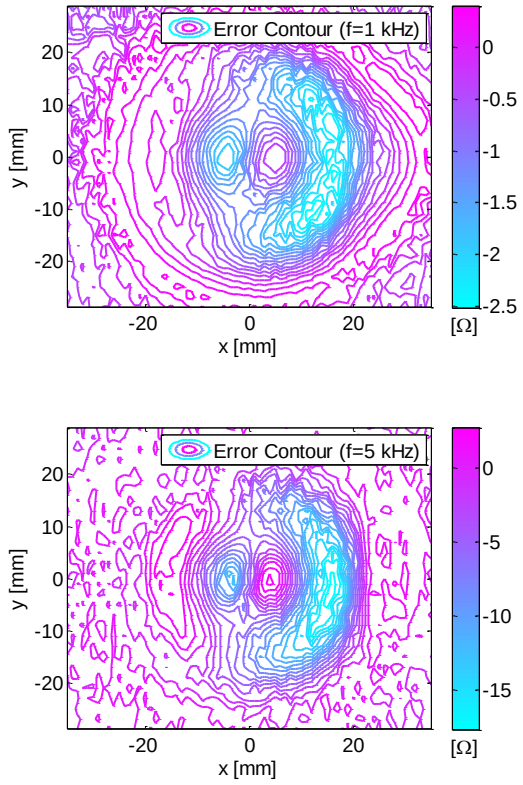

Fig. 10. Case AB - C-scan representation of the difference between the experimental and numerical impedance variation at 1 kHz and 5 kHz.

experimental impedance variation (Fig. 9) is given in Fig. 10. Also in this case the agreement is excellent: the ratio between the maximum of the difference and the maximum of the magnitude of the numerically computed impedance is 1.65×10^{-2} and 1.89×10^{-2} for 1 kHz and 5 kHz, respectively.

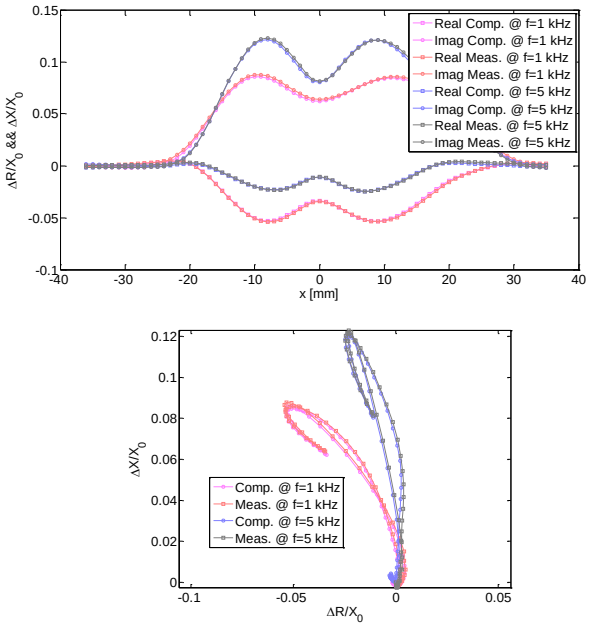

Fig. 11. Case BA – Comparison between the experimental and numerically computed data at 1 kHz and 5 kHz. top: B-scan, bottom: complex plane representation.

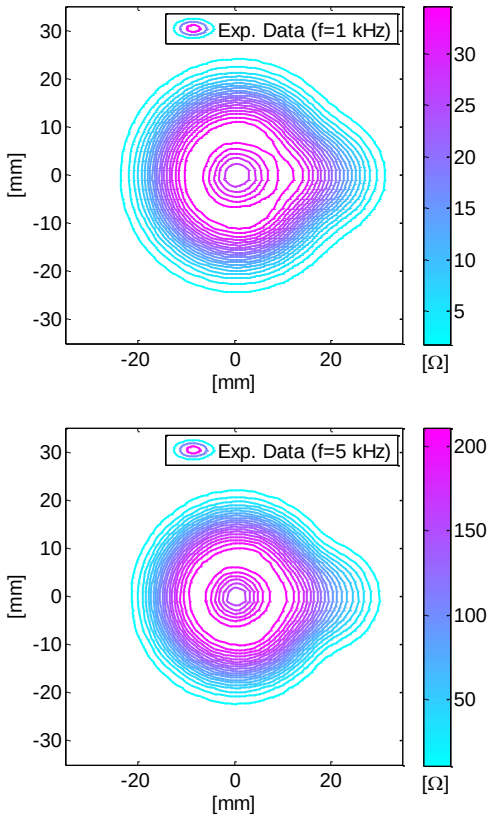

Fig. 12. Case BA - C-scan representation of the experimental impedance variation at 1 kHz and 5 kHz.

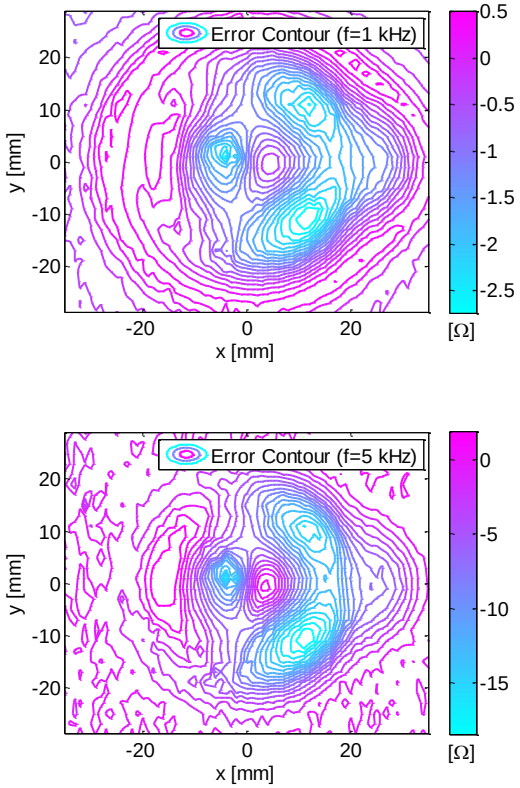

Fig. 13. Case BA - C-scan representation of the difference between the experimental and numerical impedance variation at 1 kHz and 5 kHz.

The last validation considered is relative to the Case BA, in which Plate B overlaps Plate A; the gaps between them is 70 μm. Fig. 11 shows the numerically computed data vs. the experimental one according to the coil position and also depicts the relevant complex impedance curves. A C-scan representation of the difference between the experimental (Fig. 12) and numerically computed data is given in Fig.13. Again, the agreement is excellent: the ratio between the maximum of the difference and the maximum of the magnitude of the experimental impedance is 1.94×10^{-2} and 1.37×10^{-2} for 1 kHz and 5 kHz, respectively.

VI. Conclusions

Complete experimental results were presented for a new benchmark problem in eddy current NDT. Contrary to previous benchmarks, the current problem provides quantitative and precise impedance measurements (a full C-scan of the area under interest using an XY stage). Certain geometrical aspects, like the very thin gap between the plates and the combination of two structural variations (hole(s) and crack) make the benchmark more challenging than existing TEAM Workshop ones.

The numerical simulations, carried out with an ad-hoc integral/FEM numerical model developed in the past, cross-validate the benchmark data. This numerical cross validation is appropriate/required for proposing the specific problem as a benchmark to the NDT-community. The agreement is remarkable in all considered cases. The numerical modelling/validation is non-trivial because of the multiscale nature of the problem where a thin crack, air gap and lift-off have dimensions negligible with respect to the specimen and probe. This poses challenging problems when, for instance, a standard FEM code is applied to model this configuration.

Acknowledgements

The authors thank Mr J. Martinos for his contribution to the experimental measurements. Work supported in part by the European Commission, grant agreement no. 285549, FP7.

References

[1] V.S. Cecco, G. VanDrunen and F.L. Sharp, *Eddy Current Testing*, GP Courseware, Columbia, 1987.

[2] J.S. Knopp, J.C. Aldrin and K.V. Jata, "Computational methods in eddy current crack detection at fastener sites in multi-layer structures," *NDT&E*, vol.24, no.1-2, pp.103-120, 2009.

[3] Y. Choua, L. Santandrea, Y. Le Bihan and C. Marchand, "Mesh refinement in eddy current testing with separated T-R probes," *IEEE Trans. Magn.*, vol.46, no.8, pp.2795-2798, 2010.

[4] J.R. Bowler, T.P. Theodoulidis, H. Xie and Y. Ji, "Evaluation of eddy-current probe signals due to cracks in fastener holes," *IEEE Trans. Magn.*, vol.48, no.3, pp.1159-1170, 2012.

[5] R. Miorelli, C. Reboud, D. Lesselier and T.P. Theodoulidis, "Eddy current modeling of narrow cracks in planar-layered metal structures," *IEEE Trans. Magn.*, vol.48, no.10, pp.2551-2559, 2012.

[6] R. Miorelli, C. Reboud, T. Theodoulidis, N. Poulakis and D. Lesselier, "Efficient modeling of ECT signals for realistic cracks in layered half-space," *IEEE Trans. Magn.*, vol.49, no.6, pp.2886-2892, 2013.

[7] R. Albanese and G. Rubinacci, "Finite element methods for the solution of 3D eddy current problems," Advances in Imaging and Electron Physics, P.W. Hawkes (ed.), Academic Press, vol.102, pp.1-86, 1998.

[8] Barbato, L., Petrarca, C., Rubinacci, G., Tamburrino, A. and Ventre, S., "Numerical models for composite materials in E-NDT", *Studies in Applied Electromagnetics and Mechanics*, vol.38, pp.47-54, 2014.

[9] Calvano, F., Rubinacci, G., Tamburrino, A., Vasilescu, G.-M. and Ventre, S., "Parallel MGS-QR sparsification for fast eddy current NDT simulation", *Studies in Applied Electromagnetics and Mechanics*, vol.36, pp.29-36, 2012.

[10] Rubinacci, G., Ventre, S., Villone, F. and Liu, Y., "A fast technique applied to the analysis of Resistive Wall Modes with 3D conducting structures", *J. Comput. Phys.*, vol.228, no.5, pp. 1562-1572, 2009.

[11] M. Morozov, G. Rubinacci, A. Tamburrino and S. Ventre, "Numerical models with experimental validation of volumetric insulating cracks in eddy current testing," *IEEE Trans. Magn.*, vol.42, no.5, pp.1568-1576, 2006.

[12] R. Albanese, G. Rubinacci and F. Villone, "An integral computational model for crack simulation and detection via eddy currents," *J. Comput. Phys.*, vol.152, pp.736–755, 1999.

[13] J. Martinos, T. Theodoulidis, N. Poulakis and A. Tamburrino, "A benchmark problem for eddy current nondestructive evaluation," *IEEE Trans. Magn.*, vol.50, no.2, 7026104, 2014.

[14] D.J. Harrison, L. D. Jones and S.K. Burke, "Benchmark problems for defect size and shape determination in eddy-current nondestructive evaluation," *J. NDE*, vol.15, no.1, pp.21-34, 1996.

[15] C.V. Dodd and W.E. Deeds, "Analytical solutions to eddy current probe coil problems," *J. Appl. Phys.*, vol.39, no.6, pp.2829-2838, 1968.

[16] T.P. Theodoulidis and E.E. Kriezis, *Eddy Current Canonical Problems (with Applications to Nondestructive Evaluation)*. Forsyth, GA: Techscience Press, 2006.

[17] http://www-civa.cea.fr/en/, http://www.extende.com/

[18] http://www.simposium.eu/